JOURNAL OF MATERIALS SCIENCE: MATERIALS IN ELECTRONICS **10** (1999) 571–580

Crystal growth of oxide and fluoride materials for optical, piezoelectric and other applications

T. FUKUDA, K. SHIMAMURA, V. V. KOCHURIKHIN, V. I. CHANI, B. M. EPELBAUM, S. L. BALDOCHI, H. TAKEDA, A. YOSHIKAWA
Institute for Materials Research, Tohoku University, Sendai 980-8577, Japan
E-mail: fukuda@lexus.imr.tohoku.ac.jp

High quality oxide and fluoride single crystals for optical, piezoelectric and other applications have been grown by advanced crystal growth techniques. $La_3Nb_{0.5}Ga_{5.5}O_{14}$ and $La_3Ta_{0.5}Ga_{5.5}O_{14}$ piezoelectric single crystals of size and quality comparable to $La_3Ga_5SiO_{14}$ (langasite), have been produced. The piezoelectric and device properties of the crystals were investigated. A search for new langasite-type materials was also performed. Growth conditions of $(La,Sr)(Al,Ta)O_3$ and $Ca_8La_2(PO_4)_6O_2$ single crystals are discussed. These crystals have excellent lattice matching with GaN, a promising material for optoelectronic devices. Promising optical micro-crystals—$K_3Li_2Nb_5O_{15}$, $KNbO_3$ and $Y_3Al_5O_{12}$—and new structural materials, $Al_2O_3/Y_3Al_5O_{12}$ eutectic fibers, have been grown by the micro-pulling-down (μ-PD) technique. The advantages of the μ-PD technique have been shown. Ce-doped fluoride single crystals—$LiCaAlF_6$, $LiYF_4$ and $BaLiF_3$—have been grown for solid state UV laser applications. Growth results and optical characterizations are discussed.

1. Introduction

The important role of oxide and fluoride crystals in various branches of science and technology demands a comprehensive and integrated treatment of the subject. We have carried out investigations focusing on the development of new materials for optical, piezoelectric and other applications, by using advanced crystal growth techniques. Oxide crystals are of highest importance for modern electrical and electro-optical applications in several devices. Fluoride single crystals, because of their unique properties such as large band gap, also present many advantages as optical materials.

The recent crystal growth research described in this paper involved the development of new, high-quality oxide and fluoride single crystals, and of novel crystal growth techniques. Growth of new langasite ($La_3Ga_5SiO_{14}$) single crystals for piezoelectric applications and new substrate crystals for GaN epitaxial layers, by the Czochralski (CZ) technique, is discussed. The micro-pulling-down (μ-PD) method and its application to the growth of laser, non-linear optical and structural materials are mentioned. The growth of fluoride single crystals doped with Ce for ultra-violet (UV) laser applications is also reviewed.

2. New langasite single crystals for piezoelectric applications

The recent progress of electronic technology requires new piezoelectric crystals having properties intermediate between those of quartz and $LiTaO_3$ (LT). Currently, langasite ($La_3Ga_5SiO_{14}$; LGS) crystals have received attention as new candidates for piezoelectric applications [1, 2].

The LGS crystal has the $Ca_3Ga_2Ge_4O_{14}$-type structure with the space group P321. There are four kinds of cation sites in this structure, which can be described by the chemical formula, $A_3BC_3D_2O_{14}$. In this formula, A and B represent the decahedral (twisted Thomson cube) site co-ordinated by 8 oxygens, and the octahedral site co-ordinated by 6 oxygens, respectively. C and D represent tetrahedral sites co-ordinated by 4 oxygens. Different isovalent and aliovalent substitutions in a given structure are quite interesting in themselves, and could, perhaps, also result in useful structural and physical properties.

High-quality single crystals of LGS, and its aliovalent analogs $La_3Nb_{0.5}Ga_{5.5}O_{14}$ (LNG) and $La_3Ta_{0.5}Ga_{5.5}O_{14}$ (LTG), were grown by the conventional CZ technique [3]. Fig. 1 shows the as-grown LTG single crystals of approximately 2 and 3 inches diameter. Pulling and rotation rates were 1 mm h^{-1} and 10 r.p.m., respectively.

Lattice parameter determination and chemical composition analysis were performed by the X-ray powder diffraction method and induced coupled plasma method, respectively. Lattice parameters of the grown crystals were found to be almost constant from shoulder to tail of the boules. Concentrations of each oxide, i.e. La_2O_3, Ga_2O_3, SiO_2, Nb_2O_5 and Ta_2O_5, were almost constant, within the estimated errors, throughout the crystallizing process. The uniformity of lattice parameter and chemical composition suggests that the stoichiometric composition is close to the congruently melting composition of the three compounds.

Synthesis of more than 70 chemical compositions were attempted. The incorporation of different A cations

0957–4522

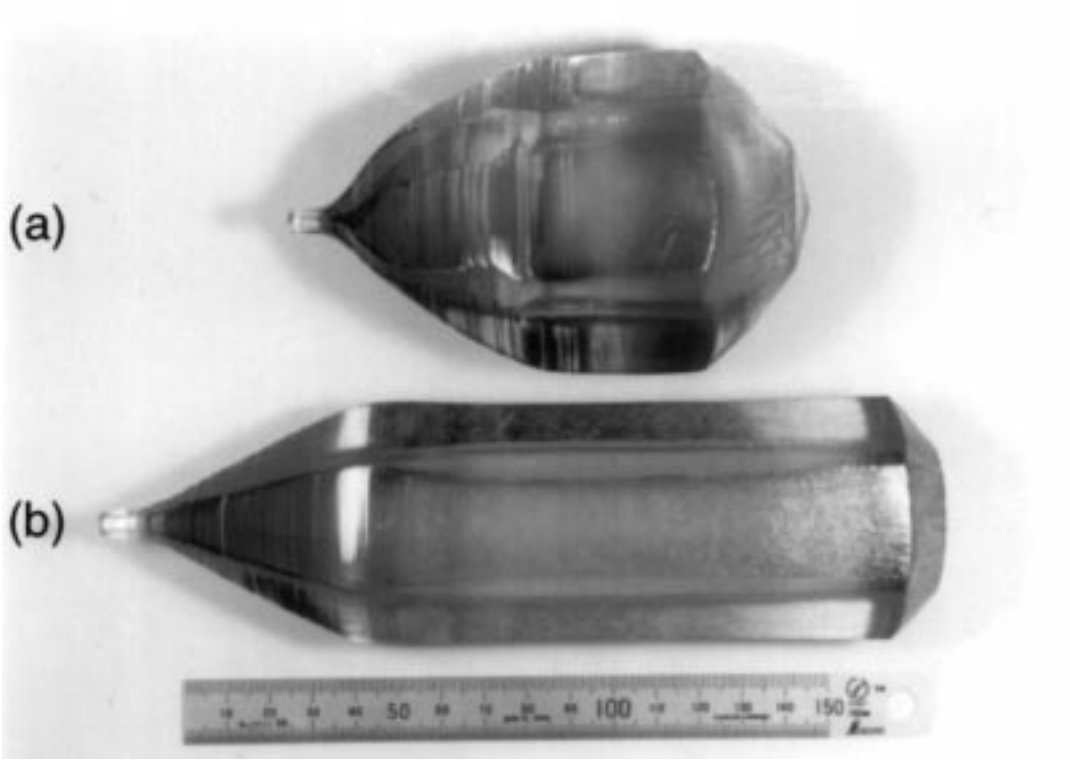

Figure 1 $La_3Ta_{0.5}Ga_{5.5}O_{14}$ single crystals 3 inches (a) and 2 inches (b) in diameter.

(Na^+, Ba^{2+}, Sr^{2+}, Bi^{3+}, Nd^{3+}, etc.) and B cations (Li^+, Mg^{2+}, Ga^{3+}, Ti^{4+}, Sb^{5+}, Mo^{6+}, etc.) into the A and B sites respectively, was studied. Materials which showed a langasite-type single phase were crystallized in fiber form by the μ-PD method, and subsequently their bulk crystals were also grown by the CZ technique. Bulk single crystals of $Sr_3Ga_2Ge_4O_{14}$, $Na_2CaGe_6O_{14}$, $Pr_3Ga_5SiO_{14}$ and $La_3Al_xGa_{5-x}SiO_{14}$ were successfully produced by the CZ technique.

Using LGS single crystals, we made monolithic-type filters (10.4 and 21.4 MHz) as seen in Fig. 2. The electrical properties of these filters include low input and output impedance, small size and low attenuation, compared with those made of quartz (see Table I).

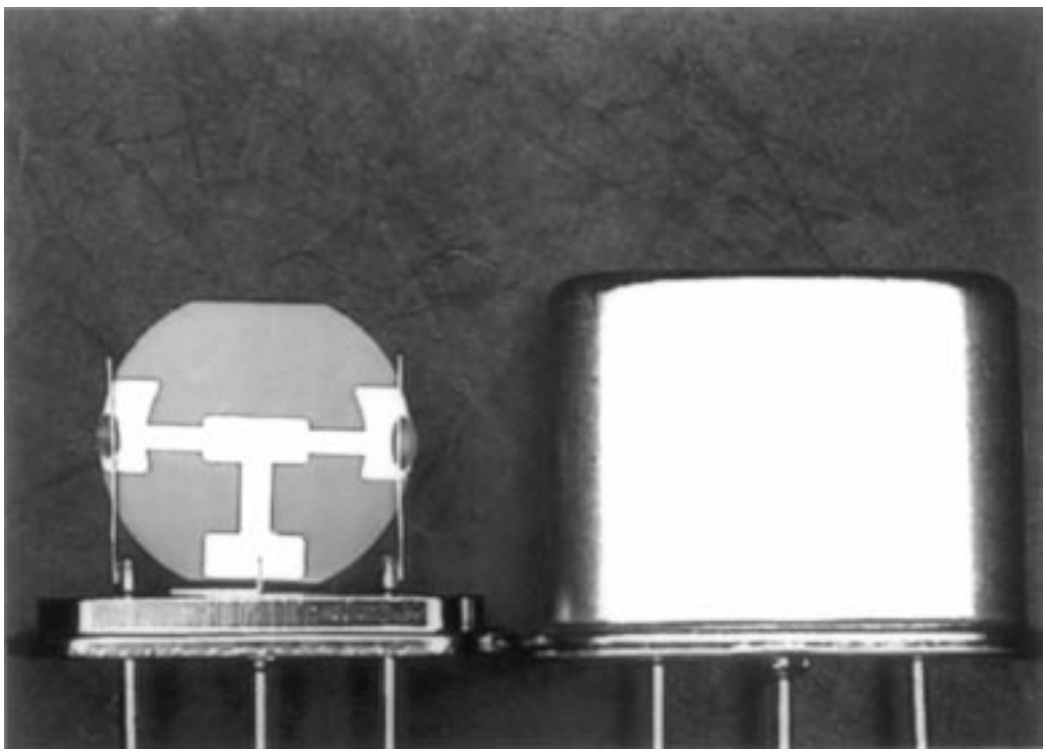

Figure 2 21.4 MHz filter made of $La_3Ga_5SiO_{14}$ single crystal (size: $6.9 \times 5.8 \times 2.2\,mm^3$).

TABLE I Electrical properties of LGS monolithic-type filters compared with quartz ones

Frequency (MHz)	Material	Passband width (3 dB) (kHz)	Attenuation (dB)	Input-output impedance (k Ω // pF)
10.7	Quartz	3 ± 15	2.5	5.5 k // − 1.0
	LGS	3 ± 15	2.0	2.5 k // 1.7
21.4	Quartz	3 ± 15	2.0	2.0 k // 0.5
	LGS	3 ± 15	2.0	800 // 4.0
	LGS	3 ± 15	2.0	1.3 k // 1.7

A 71 MHz-wide passband SMD (surface mount discrete-type) filter for the GSM (global system for mobile communication) base station was also made, which exhibited superior properties. The main features of the electrical characteristics are listed below:

1. Low input and output impedance (940 Ω/0.5 pF, versus several $k\,\Omega$ for a quartz filter);
2. Interstage coupling requires only capacitors (for a quartz filter, transfer is required);
3. Electrode gap may be wide (approximately 100 mm, versus several mm for a quartz filter).

In Table II, the characteristics of LNG, LTG and LGS are given, along with those of LT and quartz. Since LNG, LTG and LGS have no phase transitions and have lower melting point and higher hardness, the possibility of growing high-quality crystals allowing easy processing is expected to be movable. Their electromechanical coupling factors k and thermal frequency stability are between those of LT and quartz. The above characteristics indicate that LGS-family crystals are more promising materials for piezoelectric devices than lithium tetraborate ($Li_2B_4O_7$) and berlinite single crystals, which have similar piezoelectric properties [2]. $Li_2B_4O_7$ is easily soluble in all acids and bases, and readily deliquescent in air, while berlinite single crystals are difficult to grow to a large size.

Fig. 3 shows the dependence of the piezoelectric modulus $|d_{11}|$ on the lattice parameter a in the langasite-type crystals. As can be seen from the figure, an increase in lattice parameter a leads to an increase of the piezoelectric modulus $|d_{11}|$. The piezoelectric constants of LNG and LTG crystals are the largest of the langasite-type crystals studied. Therefore, we conclude that substitution of the B site is effective for improvement of the piezoelectric properties. This tendency serves as a guide for development of improved compounds of langasite-type structure.

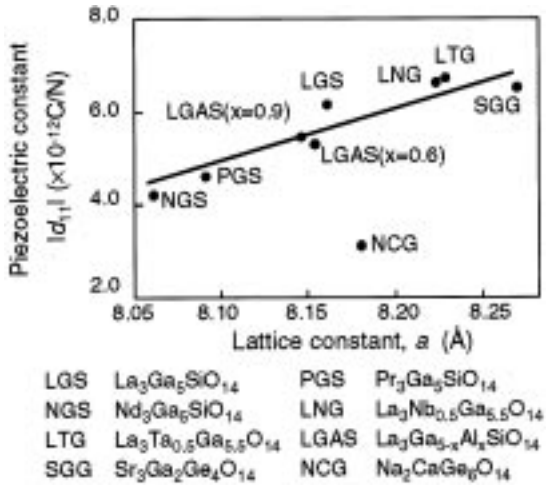

Figure 3 Piezoelectric modulus $|d_{11}|$ versus lattice parameter, a, in new crystals with langasite-type structure.

3. New substrate crystals for GaN epitaxial layers

Due to its wide direct bandgap and high thermal stability, GaN is a promising material for optoelectronic devices such as LEDs and lasers emitting in the blue to ultraviolet wavelength region, as well as for electronic devices operating at high temperatures. It has been reported that GaN layers could be grown on sapphire substrates by metal organic chemical vapour deposition (MOCVD) [4–8]. However, dislocation densities in these layers are very high, because of the large lattice mismatch between the epitaxial layers and the substrates (14–16%) [9, 10]. These dislocations have recently been shown to strongly affect the lifetime of continuous wave blue laser diodes [11]. We have found new materials (La,Sr)(Al,Ta)O_3 (LSAT) and $Ca_8La_2(PO_4)_6O_2$ (CLPA) as substrates for GaN epitaxial growth. LSAT and CLPA single crystals have been grown by the CZ technique, and lattice of parameter and crystal quality were investigated.

TABLE II Characteristics of LNG, LTG and LGS compared with those of LT and quartz

	$LiTaO_3$	LGS	LNG	LTG	Quartz
Phase transition	Exists	None	None	None	Exists
Melting point (°C)	1650	1490	1470	1500	—
Mohs hardness	5.5	6–7	6–7	6–7	7
Electromechanical coupling factor k (%)	43	15–25	~ 30	~ 30	7
Q-factor	5000	30 000–40 000	40 000–60 000	40 000–60 000	60 000–80 000
Equivalent series resistance (Ω)	—	5–10	2–5	2–5	10–20
Thermal stability (ppm) (− 20–70 °C)	200–400	~ 150	~ 150	~ 150	10–20

Figure 4 (La, Sr)(Al, Ta)O_3 single crystal grown along the ⟨1 1 1⟩ direction.

Fig. 4 shows an as-grown LSAT single crystal pulled along the ⟨1 1 1⟩ direction at a pulling and rotation rate of 1 mm h^{-1} and 10 r.p.m., respectively. The growth interface was fairly convex towards the melt. The existence of a core in the central region was clearly shown by the bright area in the cross-polarized light image. Although the growth interface at 40 r.p.m. was still convex towards the melt, the core in the central region observed in crystals grown at a crystal rotation rate of 10 r.p.m. disappeared, and the shape of the growth interface became smooth. This suggests that a higher crystal rotation speed is preferable in order to decrease the stress in the grown crystals.

Fig. 5 shows an as-grown CLPA single crystal pulled along the ⟨0 0 1⟩ direction at a pulling rate of 1.5 mm h^{-1}. There were some inclusions inside the crystals, and their distribution along the boule depended on the growth conditions. Crystals pulled at rates exceeding 2.5 mm h^{-1} always had particles of size about 10 μm, collected mainly in the core region.

The lattice parameter of the LSAT single crystal was 0.7735 nm. The lattice parameter was almost constant along the growth axis. The (1 1 1) plane of the LSAT crystals is a close-packed plane of the anion framework, which forms the primitive cubic lattice, and the ⟨1 1 1⟩ direction is the body-diagonal direction of this cubic cell. The surface structure, therefore, has hexagonal symmetry.

The lattice parameter "a_{hex}" of the LSAT (1 1 1) plane, considered as a 2-dimensional hexagonal crystal, is given by

$$a_{hex} = \sqrt{6}/3 \cdot a_{cub} \quad (1)$$

where a_{cub} is the conventional lattice parameter of the cubic crystal. Since the measured a_{cub} of LSAT was 0.7735 nm, a_{hex} was calculated to be 0.6316 nm, which was close to twice the corresponding lattice parameter of GaN (0.316 nm). The lattice mismatch was calculated to be 0.06%.

Lattice constants of CLPA (space group P63/m, hexagonal symmetry) were calculated from the powder X-ray diffraction pattern to be $a = 0.9446$ nm and $c = 0.6922$ nm. CLPA single crystals are expected to have a match with three times the lattice of GaN. The lattice mismatch between GaN and CLPA is then calculated as follows;

$$\frac{a_{GaN} - a_{CLPA}/3}{a_{GaN}} = 0.003586\ldots \quad (2)$$

i.e. 0.36%.

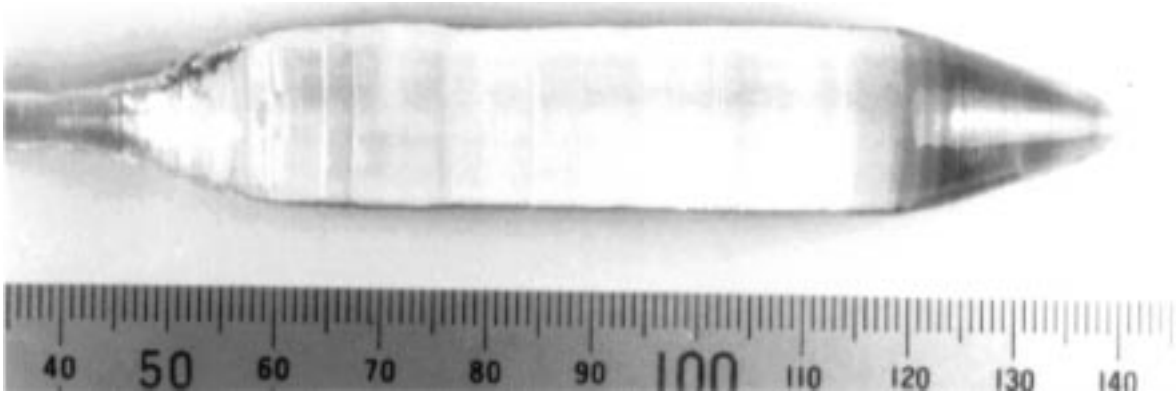

Figure 5 $Ca_8La_2(PO_4)_6O_2$ single crystal grown along the ⟨0 0 1⟩ direction.

4. Micro-crystals and fiber crystals

$K_3Li_2Nb_5O_{15}$ (KLN), which has the tungsten bronze structure, is an efficient material for frequency doubling of near-infrared (Ga,Al)As diode lasers used for recording/reading data from optical discs.

Recently, the μ-PD method was developed to produce high quality single domain KLN crystals. As-grown KLN micro-crystals were uniform in shape and were free from cracks, independent of the melt composition (Fig. 6). The highest growth rate resulting in crack-free single crystal was about 120 mm h^{-1}. The chemical composition in the crystal was uniform, and almost equal to that in the melt. Since incongruently melting materials such as KLN could be grown from the melt at high growth rates, the μ-PD method is a promising growth technique.

KLN micro-crystals showed strong second harmonic generation (SHG) blue light due to its superior non-linear optical properties. SHG properties of KLN micro-crystals grown at pulling-down rates of 12 mm h^{-1} and 80 mm h^{-1} were reported in [12]. The distribution of phase-matching wavelength along the growth axis is compared. Deviations for both crystals were about 10 nm for approximately 50 mm in length (2 nm cm^{-1}). However, SHG conversion efficiencies of these crystals were quite different. The average conversion efficiency of the crystal grown at a pulling rate of 12 mm h^{-1} was

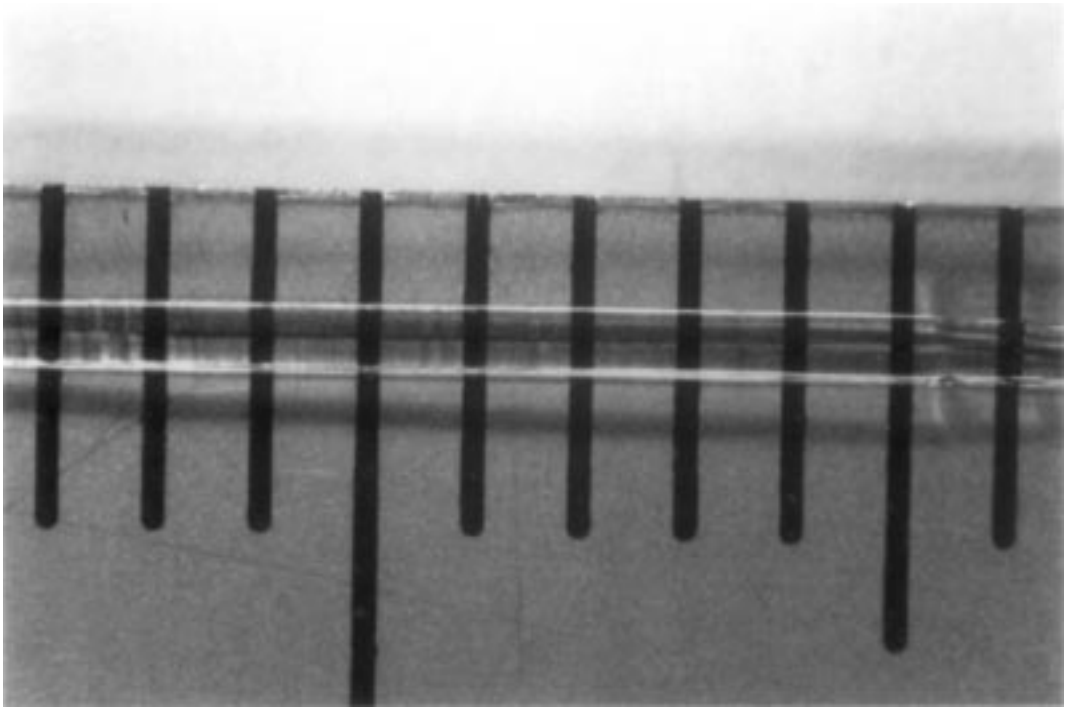

Figure 6 $K_3Li_2Nb_5O_{15}$ micro single crystal.

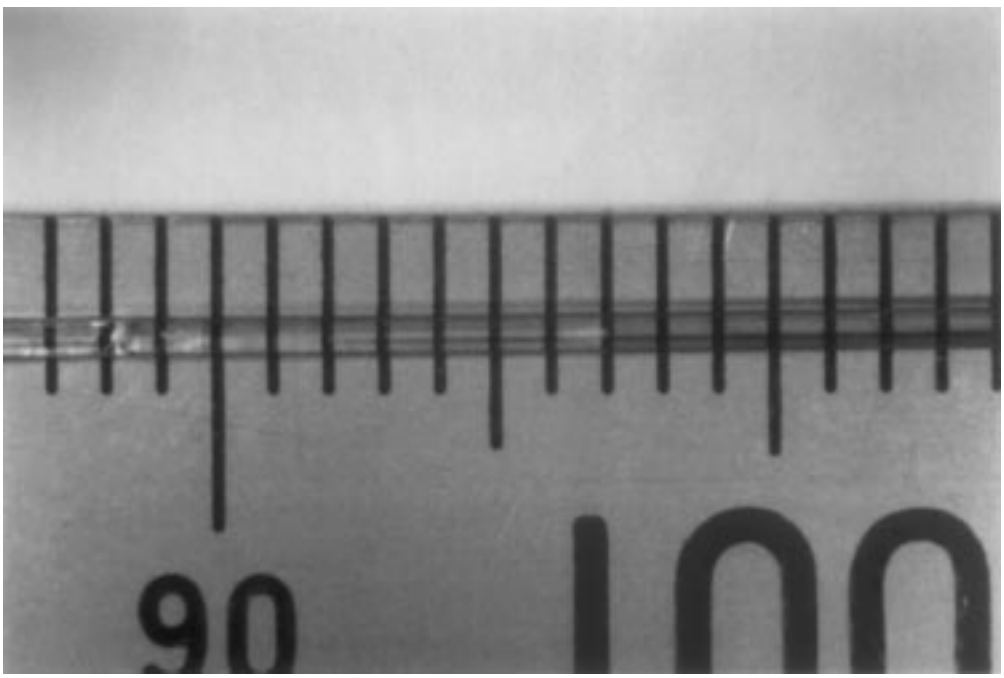

Figure 7 $KNbO_3$ micro single crystal (pulling down rate: 6 mm h^{-1}).

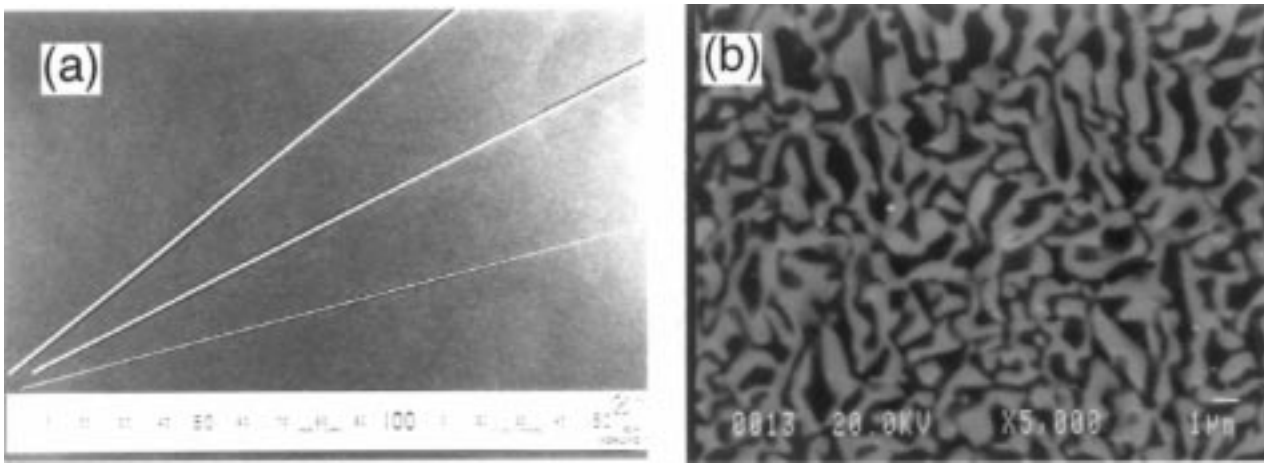

Figure 8 (a) Eutectic fibers and (b) back scattered electron image of $Al_2O_3/Y_3Al_5O_{12}$ fibers.

0.03%/W, while that of 80 mm h^{-1} was 0.006%/W. This may be related to the crystallinity or inhomogeneity.

$KNbO_3$ (KN) is also a promising material for a SHG blue laser source, since it has a large optical non-linearity ($d_{32} = 20.5$ pm V^{-1}). Incongruent melting and a phase transition during the cooling process are considered to be the main problems for the growth of high quality KN crystals. Fig. 7 shows an as-grown KN micro crystal, grown by the μ-PD method from a melt containing excess K_2O as a flux. Modification of the melt composition allowed the growth of colorless, inclusion- and crack-free SHG-active single crystals with size up to $2 \times 2 \times 15$ mm^3.

Directionally solidified ceramic eutectics are receiving strong interest because of their high structural stability up to the melting temperature. Recently, promising results were reported for $Al_2O_3/Y_3Al_5O_{12}$ (YAG) [13–15] and $Al_2O_3/GdAlO_3$ [16] systems. However, because of processing difficulties, the experimental data for oxide eutectics are still limited and often uncertain.

We have applied the μ-PD method for the growth of Al_2O_3/YAG eutectic fibers. The μ-PD method involves downward pulling of a crystalline fiber 0.1–2.0 mm in diameter through a capillary hole arranged in a crucible bottom. The μ-PD features two points important for eutectic growth: (1) a very high axial temperature gradient exists near the growth interface of the order of $3-5 \times 10^3$ °C cm^{-1} [17]. It permits high pulling rates and assures a planar interface and process stability. Secondly, (2) composition is always uniform along the fiber length, since melt convection is impossible inside the narrow capillary channel.

A high-temperature version of μ-PD employed an iridium crucible directly coupled to the r.f. power generator. A sapphire $\langle 0\,0\,0\,1 \rangle$ seed was used for growth of the eutectic fibers. The starting materials were 4 N purity Al_2O_3 and Y_2O_3 in the molar ratio of 81.3 mol % Al_2O_3 to 18.7 mol % Y_2O_3 [18].

Eutectic fibers 0.25–1.00 mm in diameter and up to 500 mm in length were grown over a range of pulling rate 0.15–10.00 mm min^{-1} (see Fig. 8). Samples of eutectic fibers grown at various pulling rates were examined using scanning electron microscopy (SEM). Several fibers were grown at a step-variable pulling rate starting from 0.15 and up to 10 mm min^{-1}. In all these experiments, the ''Chinese script'' type structure was found to possess excellent reproducibility, whereas the cellular structure was not found at all. (The microstructure of a eutectic sometimes forms the structure, which resembles a Chinese character. Such microstructure is called ''Chinese-script type'' microstructure.) The volume fraction of YAG was 0.45 ± 0.02 for all types of structure including inter-cell areas, which corresponds exactly to the theoretical value for the eutectic composition (0.44). The characteristic script size was found to be very uniform for each cross-section studied. Experimentally, the generally accepted relation $\lambda \sim v_p^{-1/2}$, where λ is interlamellar spacing of a conventional lamellar structure and v_p is the solidification rate, also applies to the script structure of the Al_2O_3/YAG system. The constant of proportionality was found to be 10, if λ has dimensions of mm and v_p mm s^{-1}. This value is large enough to allow effective microstructure control by changing the solidification rate.

The composite has been shown to have high mechanical strength up to 1800 °C, excellent oxidation resistance, high thermal stability of microstructure and thermal shock stability (Fig. 9).

Applying the same technique as described above, YAG fiber crystals with 500 μm diameter have also been grown (Fig. 10). High uniformity and high transparency have been demonstrated for these fibers.

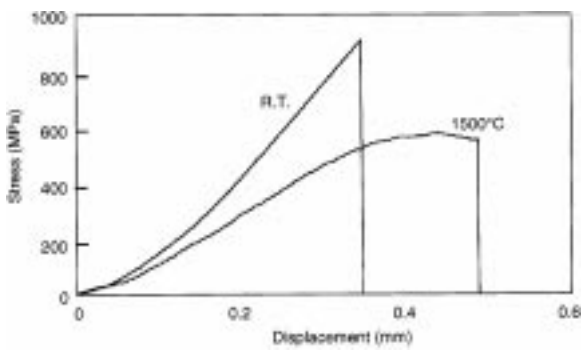

Figure 9 Tensile stress–displacement curves of $Al_2O_3/Y_3Al_5O_{12}$ eutectic fibers (grown in Ar gas atmosphere).

Figure 10 $Y_3Al_5O_{12}$ and Nd: $Y_3Al_5O_{12}$ fibers.

5. Ce-doped fluorides for UV laser applications

Coherent optical sources in the ultraviolet wavelength region are useful for many practical applications, such as medicine, semiconductor processing, optical communications and remote sensing [19]. Recently, Ce-doped $LiCaAlF_6$ (Ce:LiCAF) crystals have been reported as candidates for UV solid state lasers [20, 21]. This matrix can be directly pumped by the fourth harmonic of a Nd:YAG laser, and is suitable for tunable all-solid-state-lasers in the UV wavelength region.

We have studied Ce:LiCAF growth, under inert and fluorinating atmospheres by the CZ technique, and investigated the variation of composition and Ce^{3+} incorporation. AlF_3, CaF_2 and LiF powders, of high purity ($> 99.99\%$), were used as the starting material. CeF_3 powder ($> 99.99\%$) was used to dope the crystal in the range of 1 to 2 mol%. All crystals were grown from *a*-axis oriented seed crystals. The pulling rate was $1\,mmh^{-1}$ and the rotation rate was 10 r.p.m. The Ce^{3+} doping level in the grown crystals was measured, and the distribution coefficient of $Ce^{3+}(k_{Ce})$ in LiCAF was estimated as 0.021.

When Ce:LiCAF single crystal was grown from a stoichiometric charge under an inert atmosphere, the crystal surface was covered by white foreign substances. It is found that these substances are formed mainly of volatile fluorides, such as $LiAlF_4$, and small amounts of AlF_3 and LiF. CaF_2 was also detected in these foreign substances. The presence of oxides and oxyfluorides such as Al_2O_3, Al_4LiO_6F and CeOF was also detected.

Samples from the central part of the Ce:LiCAF crystals were used in preliminary tests of laser action. There was no coating on the parallel end faces of the crystal, which are perpendicular to the optical axis of the resonator. The fourth harmonic of a Q-switched Nd:YAG laser was used as the pumping source. Fig. 11 shows the output energies at 289 nm as a function of the absorbed pump energy at 266 nm. High-energy pulse generation from Ce:LiCAF was obtained, at a repetition rate of 10 Hz, with up to 30.5 mJ output energy and slope efficiency 39%. This laser performance is the highest ever reported for Ce:LiCAF crystals, to the authors' knowledge.

Fig. 12 shows a Ce,Na:LiCAF crystal grown under CF_4 atmosphere from a non-stoichiometric composition. An AlF_3 and LiF-rich composition was used to compensate the evaporation loss. CF_4 reacted with water in the environment, resulting in HF and CO_2, yielding a double effect of purification by elimination of water-related impurities and generating a slightly fluorinated atmosphere which also acts on oxygen-derived impurities.

The discovery of the Ce:LiCAF properties for direct UV pumping stimulated several research groups to investigate the potential of other fluoride hosts as laser

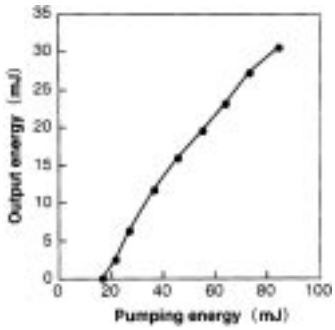

Figure 11 Input–output characteristics of Ce: $LiCaAlF_6$ laser.

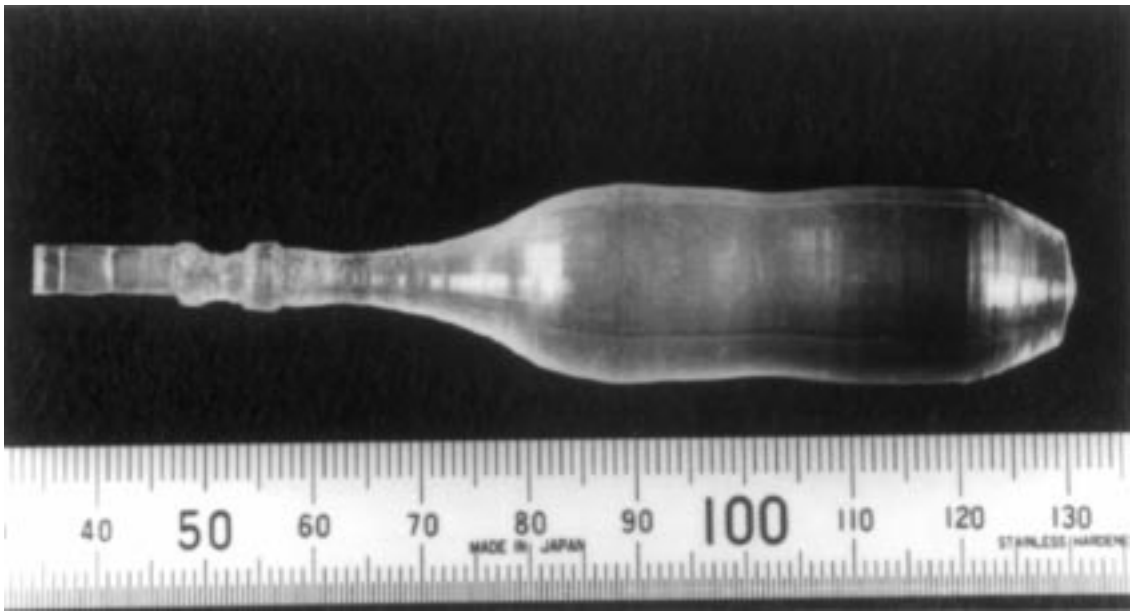

Figure 12 As-grown Ce,Na:$LiCaAlF_6$ single crystal grown under CF_4 atmosphere.

media in the UV region. Ce:$BaLiF_3$ (BLF) and Ce:$YLiF_4$ (YLF) crystals are indicated as promising candidates for a tunable UV laser.

BLF is an inverse perovskite material with cubic structure where the monovalent ion Li^+ is at the center of an F_6 octahedron and the Ba^{2+} divalent ions are in the 12-fold environment site, resulting in a different field interaction from the classic perovskite structure. YLF crystals are well known laser hosts, usually doped with rare earth ions such as Nd^{3+}, Er^{3+}, Ho^{3+} or Tm^{3+}. It is a scheelite material with tetragonal structure.

Both BLF and YLF melt incongruently, and a single crystal must be grown from a non-stoichiometric melt to avoid precipitation of other phases. We have grown large and optically high-quality crystals of Ce-doped BLF and Ce-doped YLF by the CZ method under CF_4 reactive atmosphere (Fig. 13). Commercially available YF_3, BaF_2 and LiF powders, of high purity ($> 99.99\%$), were used as the starting material. CeF_3 powder ($> 99.99\%$), was used to dope the crystal in the range of 1 to 2 mol%. The pulling rate was $1\,mmh^{-1}$ and the rotation rate was 15 r.p.m.

The measured Ce^{3+} concentration in the Ce:BLF crystal was equal to 0.011 at %. The low incorporation of Ce^{3+} ions in the BLF host is probably influenced by the difference in valence state between these ions and available substitutional sites in the crystal. Theoretically, cerium ions can be introduced in the crystal in more than one valence state with formation of compensating defects, such as vacancies, in the host lattice. The simplest measure to stabilize the valence state, and increase the Ce^{3+} concentration, is to co-dope the crystal with a second impurity or a charge-compensating additive. Fig. 14 shows a Ce,Na:BLF crystal grown under CF_4 atmosphere. The boule is transparent, without inclusions on the surface or inside.

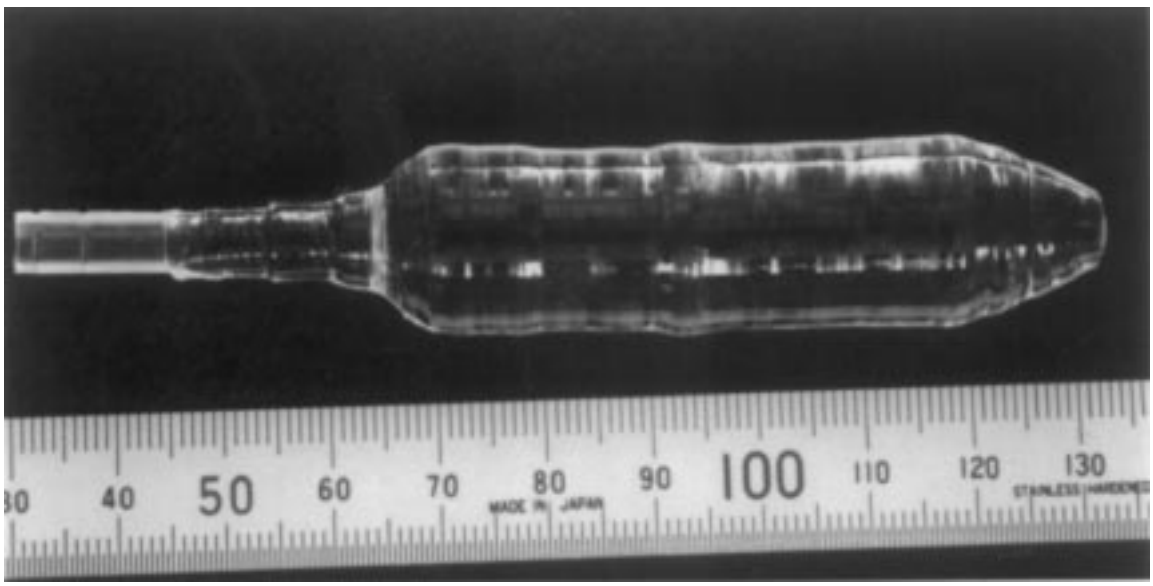

Figure 13 As-grown Ce:$YLiF_4$ single crystal.

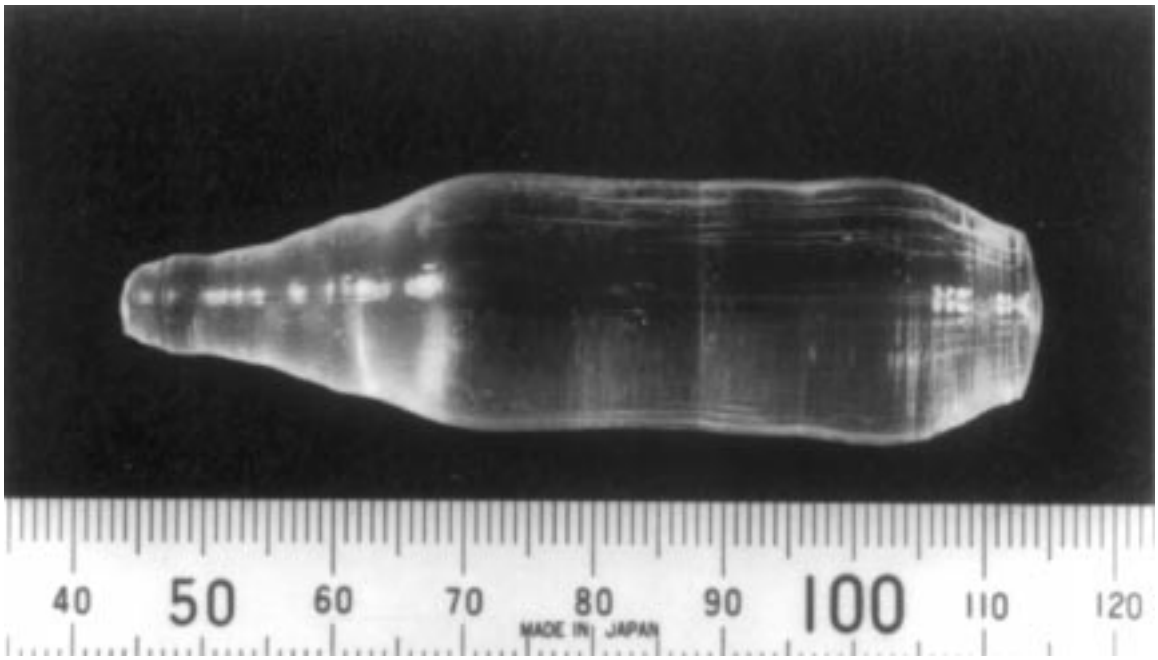

Figure 14 As-grown Ce,Na:$BaLiF_3$ single crystal.

The measurement of the Ce^{3+} concentration in co-doped crystals showed a lower Ce incorporation when compared to the singly doped one. The addition of Na^{+} ions presented an inverse result from the expected one: sodium decreased the cerium incorporation in the BLF host.

6. Summary

Various new oxide and fluoride crystals were developed. A series of new promising langasite-type materials were found. LGS, LNG and LTG single crystals with maximum size of 3 inches in diameter were successfully grown by the Czochralski technique. Prototype models of wide passband filters were prepared using these crystals. LGS, LNG and LTG single crystals were shown to have superior piezoelectric properties compared to other compounds with properties intermediate between those of quartz and LT. Detailed study of the CZ crystal growth process and characterization of the grown crystals allowed the design of new materials for optical applications, such as LSAT and CLPA, having high potential as substrates for the growth of high-quality GaN epitaxial layers with low dislocation density. Micro-crystals are recognized as possessing superior properties for use in a new generation optical system. Promising non-linear optical materials such as KLN and KN micro-crystals were grown. By applying the high-temperature μ-PD technique, directionally-solidified eutectic Al_2O_3/YAG fibers and YAG fibers were also grown. A study of purification and crystal growth processes resulted in the growth of large crystals of Ce,Na:LiCAF, Ce:BLF and Ce:YLF with good optical quality. High-energy pulse generation (30.5 mJ) was obtained from a Ce:LiCAF laser. This laser performance proves that Ce:LiCAF is a promising material for high-energy UV pulse generation combined with a high-power, Q-switched Nd:YAG laser.

Acknowledgements

The authors would like to acknowledge and thank Associate Professor Dr. S. Durbin and the members of the Fukuda Laboratory of the Institute for Materials Research, Tohoku University. They are also indebted to Mr J. Sato (TDK Corporation), Mr H. Kawanaka (Victor company of Japan, Ltd.), Mr S. Murakami (KYOCERA Corporation), Mr H. Tabata (NICHIA Chemical Industries, Ltd.), Dr K. Imai (NGK Insulators) for their many contributions.

References

1. I. M. SILVESTROVA, YU. V. PISAREVSKY, V. V. BEZDELKIN and P. A. SENYUSHENKOV, Proceedings of the 1993 IEEE International Frequency Control Symposium, p. 351.
2. J. DETAINT, J. SCHWARTZEL, A. ZARKA, B. CAPELLE, J. P. DENIS and E. PHILIPPOT, Proceedings of the 1994 IEEE International Frequency Control Symposium, p. 58.
3. K. SHIMAMURA, H. TAKEDA, T. KOHNO and T. FUKUDA, *J. Cryst. Growth* **163** (1996) 388.
4. S. NAKAMURA, T. MUKAI and M. SENOH, *Appl. Phys. Lett.* **64** (1994) 1687.
5. S. NAKAMURA, M. SENOH, N. IWASA and S. NAGAHAMA, *Jpn. J. Appl. Phys.* **34** (1995) L797.
6. S. NAKAMURA, M. SENOH, S. NAGAHAMA, N. IWASA, T. YAMADA, T. MATSUSHITA, H. KIYOKU and Y. SUGIMOTO, *ibid.* **35** (1996) L74.
7. I. AKASAKI, H. AMANO, S. SATO, H. SAKAI, T. TANAKA and M. KOIKE, *ibid.* **34** (1995) L1517.
8. H. MORKOC, S. STRITE, G. B. GAO, M. E. LIN, B. SVERDLOV and M. BURNS, *J. Appl. Phys.* **76** (1994) 1363.
9. S. D. LESTER, F. A. PONCE, M. G. CRAFORD and D. A. STEIGERWALD, *Appl. Phys. Lett.* **66** (1995) 1249.
10. M. OSINSKI and D. L. BARTON, Proceedings of the 1996 International Symponium on Blue Laser and Light Emitting Diodes, p. 217.
11. H. AMANO, N. SAWAKI, I. AKAZAKI and Y. TOYODA, *Appl. Phys. Lett.* **48** (1986) 353.
12. K. IMAI, M. IMAEDA, S. UDA, T. TANIUCHI and T. FUKUDA, *J. Cryst. Growth* **177** (1997) 79.

13. T. A. PARTHASARATHY, T. I. MAH and L. E. MATSON, *J. Am. Ceram. Soc.* **76** (1993) 29.
14. Y. WAKU, N. NAKAGAWA, H. OHTSUBO, Y. OHSORA and Y. KOHTOKU, *J. Jpn. Inst. Metals* **59** (1995) 71.
15. Y. WAKU, H. OHTSUBO, N. NAKAGAWA and Y. KOHTOKU, *J. Mater. Sci.* **31** (1996) 4663.
16. Y. WAKU, N. NAKAGAWA, T. WAKAMOTO, H. OHTSUBO, K. SHIMIZU and Y. KOHTOKU, *Nature* **389** (1997) 49.
17. S. UDA, J. KON, J. ICHIKAWA, K. INABA, K. SHIMAMURA and T. FUKUDA, *J. Cryst. Growth* **179** (1997) 567.
18. D. VIECHNICKI and F. SCHMID, *J. Mater. Sci.* **4** (1969) 84.
19. N. SARUKURA, M. A. DUBINSKII, Z. LIU, V. V. SEMASHKO, A. K. NAUMOV, S. L. KORABLEVA, R. Y. ABDULSABIROV, K. EDAMATSU, Y. SUZUKI, T. ITOH and Y. SEGAWA, *IEEE J. Sel. Topics Quantum Electron.* **1** (1995) 792.
20. M. A. DUBINSKII, V. V. SEMASHKO, A. K. NAUMOV, R. Y. ABDULSABIROV and S. L. KORABLEVA, *Laser Phys.* **3** (1993) 216.
21. C. D. MARSHALL, S. A. PAYNE, J. A. SPETH, W. F. KRUPKE, G. J. QUARLES, V. CASTILLO and B. H. T. CHAI, *J. Opt. Soc. Am. B.* **11** (1994) 2054.

Received 4 January
and accepted 12 February 1999